

LABORATORY SIMULATION OF PHOTOCHEMICALLY REACTING ATMOSPHERIC BOUNDARY LAYERS: A FEASIBILITY STUDY

MARTIN I. HOFFERT

Institute for Space Studies, Goddard Space Flight Center, NASA, New York, New York 10025, U.S.A.

WALTER G. HOYDYSH

Environmental Research Laboratories, New York University, Bronx, New York 10453, U.S.A.

SULTAN HAMEED

Institute for Space Studies, Goddard Space Flight Center, NASA, New York, New York 10025, U.S.A.

and

SERGEJ A. LEBEDEFF

Computer Sciences Corporation, New York, New York 10025, U.S.A.

(First received 18 December 1973 and in final form 17 April 1974)

Abstract—Using a smog-chamber-validated computer model for the photochemical kinetics of C_3H_6/NO_x systems, it is shown that by proper choice of reactant concentrations and light intensities, the reaction rates can be sufficiently accelerated to yield ozone formation times of 30 s or less. These conditions permit study of photochemical smog formation in wind-tunnel-simulated atmospheric boundary layers with turbulent-mean flow velocities of $1/3 \text{ m s}^{-1}$ over test sections 10 m long. Advantages and limitations of this technique for studying inhomogeneous mixing in reacting flows, the influence of complex topography and temperature inversions, and validation studies of urban air pollution dispersion models, are discussed in some detail. The method is particularly attractive for fundamental studies of nonlinear interactions in chemically reacting turbulent shear flows under controlled conditions unobtainable in real atmospheres. A specific experiment is proposed wherein C_3H_6/NO_x mixtures are injected into a wind tunnel boundary layer in a test section irradiated by NO_2 -photolyzing ultraviolet lamps which drive the smog-forming reactions.

INTRODUCTION

Since it was first detected in Southern California over 30 y ago, photochemical smog—a condition associated with sunlight-induced chemical reactions of hydrocarbon (HC) and nitrogen oxide ($NO_x = NO + NO_2$) emissions, primarily from automobiles—has become increasingly important from the standpoint of pollution control. Not only are HC and NO_x recognized pollutants in themselves (*Air Quality Criteria for Hydrocarbons*, 1970; *Air Quality Criteria for Nitrogen Oxides*, 1971), but the photochemical oxidants formed in the atmosphere by their reactions, particularly ozone (O_3) and peroxyacetyl nitrates (PAN), are also noxious (*Air Quality Criteria for Photochemical Oxidants*, 1970). Furthermore, as aerometric data for these species has accrued—for example, from the Continuous Air Monitoring Project (CAMP) of the U.S. Environmental Protection Agency (Larson, 1971)—it has become abundantly clear that photochemical oxidants are not confined to the Los Angeles Basin, but are present in significant concentrations over other major cities which rely on the automobile for transportation.

Clearly, air chemistry plays a major role in determining ambient levels of HC, NO_x and photochemical oxidants, but to understand the relationship between the distribution of these pollutants over a highway, a power plant or an entire city, and the distribution of their emission sources, it is necessary to also account for advective transport and turbulent mixing in the atmospheric boundary layer. Thus far, the *coupling* of all these processes has been studied only theoretically using computer models of the reacting flow of pollutants over cities (or parts of cities) subject to prescribed solar flux, meteorology and source emission distributions (Lamb and Seinfeld, 1973; Hoffert, 1972; Eschenroeder and Martinez, 1972; Seinfeld *et al.*, 1972). Generally speaking, these models are approximate solutions to the time-dependent conservation of mass equations for multicomponent gas mixtures in a turbulent field, where the chemical source terms in these equations are checked independently in the *absence* of fluid dynamic effects against time-histories of HC, NO, NO₂, O₃ and PAN observed in laboratory smog chambers; the philosophy being that these kinetic schemes can be combined with transport processes later, in models which, suitably "tuned", will replicate pollution concentration fields over actual urban regions. In principle, such validated dispersion models could serve as valuable tools in assessing the outcomes of alternate pollution control strategies, in devising rational air monitoring systems, in land use studies and highway planning, and in cost/benefit optimization.

It has unfortunately proven difficult and expensive to validate photochemical smog dispersion models for several reasons: First, there is the problem that the chemical kinetic schemes are computationally cumbersome even in the case of a single reactive hydrocarbon whereas urban atmospheres typically contain mixtures of large numbers of hydrocarbons, each of which differs in the details of its photooxidation. This has led to a number of approximations associated with the chemistry of real polluted air which are difficult to check even in the absence of transport. Secondly, transport processes in urban atmospheres proceed under conditions of complex topography and wind fields which are often chaotic over spatial resolution scales required for modelling. Finally, there are uncertainties as to the proper form of the chemical source terms in a turbulent flow field which have been touched on theoretically (Donaldson and Hilst, 1972; Lamb, 1973) but remain unresolved for lack of experimental confirmation. The result is that when model predictions are compared with field observations from air monitoring networks, it is not clear what factors the differences can be attributed to. In turn, this renders the tuning phase of model development a largely empirical art and necessarily compromises the overall confidence level of the model.

We wish to propose an experimental approach to the study of photochemical smog in atmospheric boundary layers which we believe could resolve some of these difficulties. The basic idea is to generate photochemical smog species in the turbulent shear layer over a wind tunnel test section irradiated by u.v. light, and to measure their distributions with suitable instrumentation. This paper deals with the feasibility and applicability of such experiments.

FLUID DYNAMIC SIMILITUDE

For chemically *inert* pollutants, wind-tunnel scale modelling of dispersal patterns from isolated and distributed emission sources is a well-established simulation technique, particularly effective when topography and/or urban roughness effects (difficult or impossible to capture in purely computational models) exert an important influence on the flow field (Cermak, 1971; Sundaram *et al.*, 1972; Hoydysh and Ogawa, 1972a, 1972b). The successful

scaling of such experiments to determine the velocity, temperature and concentration fields over real power plants, highways, urban complexes, etc. derives from the formal analogy which exists between laboratory-scale boundary layers and full-scale atmospheric surface layers when certain fluid dynamic *similarity* parameters are matched for the two flows. Under the proper conditions, the laboratory experiment serves as a kind of analog computer replicating the real flow field in a scaled-down, but controllable, manner.

For layers of thickness δ , mean velocity u_0 and mean temperature T_0 , containing air of density ρ , kinematic viscosity ν , thermal conductivity k and constant-pressure specific heat C_p , these similarity parameters—derivable from nondimensionalized forms of the boundary-layer momentum, energy and mass conservation equations (Snyder, 1972)—include the Reynolds number $Re \equiv u_0\delta/\nu$, the Prandtl number $Pr \equiv \nu/\kappa$ and the Schmidt number $Sc_i \equiv \nu/D_{ij}$ when *molecular transports* are important, where $\kappa = k/(\rho C_p)$ is the thermal diffusivity, and D_{ij} is the binary diffusion coefficient between species i and j ; the Rossby number

$$Ro \equiv u_0/(\delta\Omega)$$

when *Coriolis* forces are important, where Ω is the angular velocity; and the Richardson number

$$Ri \equiv \frac{g}{T} \cdot \frac{(\partial T/\partial z)}{(\partial u/\partial z)^2} \simeq \frac{g\delta\Delta T}{u_0^2 T_0}$$

when thermal stratification or *buoyancy* forces are important, where g is the gravitational acceleration, $\partial u/\partial z \simeq u_0/\delta$ is the vertical shear, ΔT is the temperature difference across the layer and $\partial T/\partial z \simeq \Delta T/\delta$ is the temperature gradient (in the atmospheric boundary layer this is replaced by the *potential temperature gradient*, $\partial\theta/\partial z = \partial T/\partial z + \Gamma$, where $\Gamma = -g/C_p \simeq -9.8^\circ\text{C km}^{-1}$ is the adiabatic lapse rate—note also that nearly all atmospheric boundary-layer theories embody the Boussinesq approximation: $\Delta T/T_0 \ll 1$). In simulations of buoyant plume rise, the Froude number $Fr \equiv Ri^{-1/2}$ is often used as an alternate stratification parameter.

Generally speaking, the atmospheric boundary layer is in a state of turbulent motion wherein the velocity vector, the temperature and the concentration of a generic (i th) chemical specie are expressible as $\mathbf{U} = (u, v, w) = (\bar{u} + u', \bar{v} + v', \bar{w} + w')$, $T = \bar{T} + T'$ and $X_i = \bar{X}_i + X_i'$, where the overbar denotes the turbulent-mean and the “prime” denotes the instantaneous fluctuation about the mean, as indicated. Typically, a turbulent boundary layer is created in wind-tunnel simulations by operating at Reynolds numbers high enough to induce transition (with the aid of a trip mechanism if necessary). In turbulent flow, the diffusion or mixing of mass, momentum and energy is accomplished by turbulent eddies which are far more effective in redistributing these quantities than molecular diffusion. Furthermore, the energy-containing eddies characteristically have length scales over which laminar viscosity is not a factor (see later discussion). Accordingly, under post-transition, “mature turbulence” conditions the flow field becomes *Reynolds-number-independent* (Snyder, 1972), and momentum, for example, is exchanged in the vertical direction by the turbulent eddy viscosity

$$\epsilon_z = \frac{-\overline{u'w'}}{\partial\bar{u}/\partial z} \quad (1)$$

which is usually much greater than the kinematic (molecular) viscosity ν in both wind-tunnel and geophysical boundary layers. The transports of sensible heat and species mass

are also enhanced in a similar way, a feature which is generally characterized by taking the *turbulent* Prandtl and Schmidt numbers

$$Pr_T \equiv \frac{\epsilon_z}{T'w' / (\partial T / \partial z)}, \quad Sc_{i,T} \equiv \frac{\epsilon_z}{X_i'w' / (\partial X_i / \partial z)}$$

of order or equal to unity.

It is not possible to simulate finite Rossby number Coriolis effects in conventional wind tunnels (these can be modelled to some extent in rotating tank or so-called "dishpan" experiments). Fortunately, this is not an important constraint in the present context because the constant-flux or Monin-Obukov surface layer, extending some 10-100 m upwards from the surface in the real atmosphere (but below the Ekman layer part of the planetary boundary layer where Coriolis forces play a role), is a region where HC and NO_x emissions exist in high enough concentrations to form appreciable smog layers. This layer, characterized by a constant turbulent flux of momentum expressed as the friction velocity $u^* \equiv (-\overline{u'w'})^{1/2}$ and a constant flux of sensible heat $H \equiv \rho C_p \overline{T'w'}$, both in the vertical direction, can, in fact, be simulated rather well in a wind tunnel. While the planetary boundary layer, of the order of 1 km thick, is often capped by an elevated temperature inversion, the turbulent region below including the surface layer part exists in varying states of thermal stratification. For the neutrally stable ($Ri = 0$) case the heat flux vanishes and the surface layer eddy viscosity takes the form

$$\epsilon_z = \tilde{k} u^* z,$$

where $\tilde{k} \simeq 0.4$ is von Karman's constant and z is the vertical coordinate. Substituting this into (1) and integrating gives the familiar logarithmic *law of the wall* for the turbulent-mean velocity profile,

$$\bar{u}(z) = (u^*/\tilde{k}) \ln(z/z_0),$$

where z_0 is the height of an aerodynamic roughness element associated with surface topography. Strictly speaking, in order to properly scale topography effects on the surface layer it is necessary to match the ratio z_0/δ (Jensen, 1958).

The degree of thermal stratification and therefore the stability of the constant-flux surface layer is characterized by the Monin-Obukhov length scale $L = -u^{*3} \rho C_p \bar{T} / (\tilde{k} g H)$ which can, in turn, be related to the Richardson number (see, e.g. Hoffert, 1972). The Pasquill stability classes commonly used to correlate stratification effects in air pollution dispersion problems correspond to Richardson numbers ($a z = 2$ m in the range of $Ri = -1.0$ ($L = -3$ m) for extremely unstable conditions to $Ri = 0.11$ ($L = 35$ m) for moderately stable conditions. Cermak (1971) has shown that Richardson numbers in the range $-0.5 \leq Ri \leq 0.5$ are readily obtainable in wind tunnel simulations. This is sufficient for reproducing most of the conditions commonly encountered in urban atmospheres. For the general case of non-neutrally-stratified atmospheres, the surface-layer profiles of turbulent-mean velocity and temperature are given by (Monin and Yaglom, 1971),

$$\bar{u}(z) = (u^*/\tilde{k}) [\ln(z/z_0) - \psi(z/L)], \quad (2a)$$

$$\bar{T}(z) - \bar{T}_0 = T^* [\ln(z/z_0) - \psi(z/L)], \quad (2b)$$

where $\bar{T}_0 = \bar{T}(z_0)$ is the temperature ($a z = z_0$), $T^* = -H / (\rho C_p \tilde{k} u^*)$ is a reference temperature and ψ is a universal function of the vertical coordinate normalized to the Monin-Obukov length (again, for applications to the atmospheric surface layer, the temperature

is replaced by the *potential temperature* $\theta \equiv T(1000/p)^{R/C_p}$ where p is the pressure in mbars and R is the gas constant for air). There is ample evidence that boundary layers satisfying the profile laws of (2a and b) can be generated on laboratory scales (Cermak, 1971; Sundaram, 1972; Counihan, 1973; Cook, 1973).

The distribution of energy in turbulent fluctuations over the spectrum of eddy scale sizes—or their reciprocals expressed as wavenumbers K —is another factor which must be assessed in scaling the atmospheric boundary layer. Over the equilibrium range of turbulence, the cascading of energy from the mean shear flow to turbulent fluctuations at higher wavenumbers can depend only on the viscous dissipation rate per unit mass of order $\epsilon \sim u_0^3/\delta$ and the kinematic viscosity ν (Tennekes and Lumley, 1972). The one-dimensional power spectrum of, say, longitudinal velocity fluctuations $f(K)$ which has the units of length, can, following the dimensional arguments of Kolomogorov (1941), be expressed in the normalized form

$$\frac{\overline{u'^2 f(K)}}{v^2 \eta} = \phi(K\eta)$$

where $v \equiv (\nu\epsilon)^{1/4}$ and $\eta \equiv (\nu^3/\epsilon)^{1/4}$ are the Kolomogorov velocity and length scales, respectively. Over the inertial subrange of the turbulent spectrum—strictly speaking, only when $K\delta \rightarrow \infty$, $K\eta \rightarrow 0$ and $Re \rightarrow \infty$ —the decay law $\phi \sim (K\eta)^{-5/3}$ was predicted by Kolomogorov. Cermak (1971) showed that longitudinal spectra obtained in both wind tunnel and geophysical flows exhibit this scaling and possess a very nearly $-5/3$ power decay law in the range $10^{-3} < K\eta < 10^{-1}$. A wavenumber normalization by δ should also exhibit a $(K\delta)^{-5/3}$ law [or a $(K\delta)^{-2/3}$ law if $f(K)$ is multiplied by $K\delta$] over the inertial subrange but here the point at which the spectrum departs from this behavior because of molecular-scale diffusion (i.e. at the beginning of the viscous dissipation range) depends, in principle, on the Reynolds number. But Sundaram *et al.* (1972) considering measured power spectra in both longitudinal and vertical directions with essentially this type of normalization found that atmospheric and wind tunnel-simulated surface layers have indistinguishable spectral properties over the range $10^{-2} \leq K\delta \leq 10$ where most of the energy is concentrated. This happens despite the Reynolds number differences because the Reynolds number in both cases is sufficiently high to render the viscous subrange relatively unimportant. These are important results because they imply spectral as well as bulk transport similitude and lend further credence to wind tunnel simulations of turbulence effects in *reacting* atmospheric flows.

PHOTOCHEMICAL SIMILITUDE

For applications to the proposed wind tunnel studies of *photochemically reacting* surface layers, all of the foregoing fluid dynamic similarity requirements apply, but additional constraints are imposed by the chemistry; namely, that reaction times must be comparable to test-section residence times and that the concentration fields generated over the test section should, in some meaningful sense, be scalable to real atmospheric conditions. In this section we discuss these requirements and the feasibility of satisfying or approximating them for photochemical smog reacting systems.

To make the analysis more concrete, consider the wind-tunnel generation of photochemical smog in an approximately two-dimensional (transversely homogeneous) turbulent shear layer by slot injection of an HC/NO_x mixture near the inlet, from the lower surface,

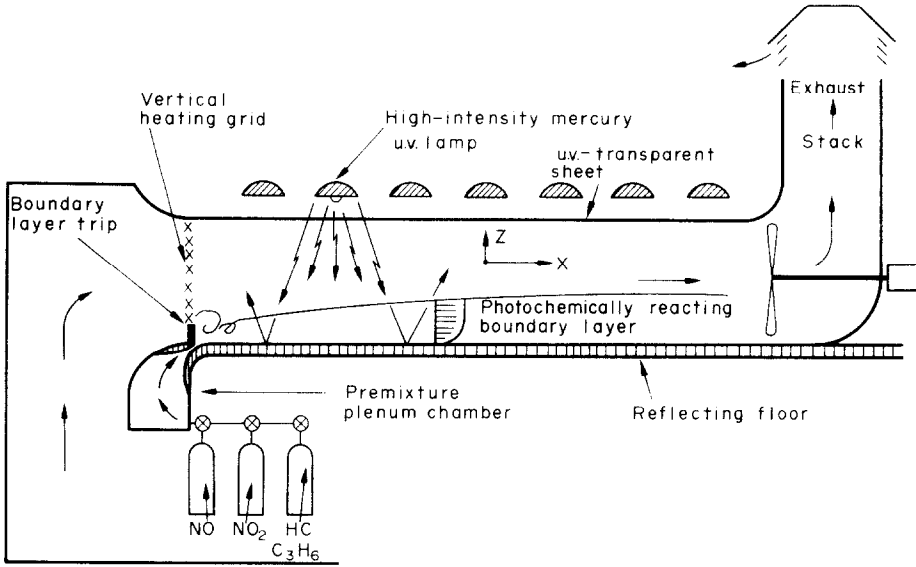


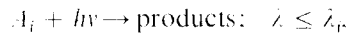
Fig. 1. Schematic diagram of photochemical smog wind tunnel experiment.

and perpendicular to the axis, x , of a test section irradiated by artificial (simulated solar) ultraviolet light sources (Fig. 1). This set-up could, for example, represent smog formation from a highway in a crosswind. Under steady-state conditions, the turbulent-mean concentration field in this simulated surface layer is described by

$$u \frac{\partial \bar{X}_i}{\partial x} = Sc_{i,T}^{-1} \times \frac{\partial}{\partial z} \left(\epsilon_z \frac{\partial \bar{X}_i}{\partial z} \right) + \bar{X}_i, \quad (3)$$

where $\bar{X}_i = \bar{X}_{i,p} + \bar{X}_{i,c}$ is the chemical source term for species i , $\bar{X}_{i,p}$ being the contribution from photolytic and $\bar{X}_{i,c}$ the concentration from collisional chemical reactions. The chemical source term for species i —a function of the light intensity and the concentrations of other (j th) species—is worth examining in greater detail in the context of the present problem.

In a general photodissociation reaction,



the concentration of species i is destroyed at a rate

$$\dot{X}_{i,p} = -J_i X_i \quad (4)$$

where the unimolecular photolysis rate J_i is expressible as

$$J_i = (hc)^{-1} \int_0^{\lambda_i} \lambda I_\lambda \sigma_{\lambda i} \Phi_{\lambda i} d\lambda, \quad (5)$$

where λ is the wavelength of light in Å ($1 \text{ Å} = 10^{-10} \text{ m}$, λ_i is a cut-off wavelength above which light is insufficiently energetic to dissociate species i), I_λ is the light intensity at wavelength λ in $\text{W}\cdot\text{m}^{-2}\cdot\text{Å}^{-1}$, $\sigma_{\lambda i}$ is the photodissociation cross-section in m^2 and $\Phi_{\lambda i}$ is the quantum yield (dimensionless) of species i at wavelength λ , $d\lambda$ is the differential wavelength

in m, $h = 6.625 \times 10^{-34}$ J-s is Planck's constant and $c = 3.00 \times 10^8$ m s⁻¹ is the velocity of light *in vacuo*. Accordingly, J_i in (5) has the dimensions of s⁻¹ although it is often given in the air pollution literature in min⁻¹ (note that 1 W/J = s⁻¹). For nitrogen dioxide (NO₂)—by far the most photochemically active substance in smog via the NO₂ + $h\nu \rightarrow$ NO + O reaction and the key to the entire process of hydrocarbon photooxidation—Leighton (1961) quotes a value of $J_{\text{NO}_2} \simeq 0.33$ min⁻¹ at a solar zenith angle of 45° over the u.v. absorption band $2900 \leq \lambda \leq 3850$ Å. In this regime $\sigma_{\lambda, \text{NO}_2}$ is of the order 10⁻²² m² and $\Phi_{\lambda, \text{NO}_2}$ (the ratio of photons absorbed to NO or O-atom particles produced) is very nearly unity.

In laboratory smog chambers, there is usually some effort made to select a light source which approximates the u.v. solar spectrum and matches the sunlight-induced values of the NO₂ photolysis rate. For example, we have in Fig. 2 compared the normalized photon flux

$$F(\lambda) \equiv \lambda I_{\lambda} / I_0 \quad (6)$$

in the range $3000 \leq \lambda \leq 4200$ Å, where $I_0 = \int_0^{\infty} I_{\lambda} d\lambda$, of a fluorescent bulb commonly used in smog chamber work—i.e. GE F40 BLB, computed from published spectral properties of this light source (*Black Light*, 1971)—with the solar u.v. photon flux distribution in the lower atmosphere estimated by Leighton (1961) at a solar zenith angle of 40°. For normalization purposes we have taken $I_0 = 100$ W-m⁻², about 7 per cent of the solar constant $S_0 \simeq 1400$ W-m⁻², as a characteristic integrated solar radiation intensity over this range. This bulb emits primarily in the u.v. at a characteristic wavelength of

$$\lambda^* \equiv \int_0^{\infty} F(\lambda) d\lambda \simeq 3560 \text{ Å.} \quad (7)$$

Also, it is known from many previous studies (e.g. Dodge and Bufalini, 1972) that arrays of GE F40 BLB lamps can easily generate photolysis rates J_{NO_2} in the range of 0.35–0.50 min⁻¹ in irradiated smog chambers, a good approximation to values generated by the midday sun.

It follows from (5, 6 and 7) that unimolecular photolysis rates scale linearly with I_0 , that is

$$J_i = a_i I_0 \quad (8)$$

where $a_i \equiv (hc)^{-1} \int_0^{\infty} F(\lambda) \sigma_{\lambda i} \Phi_{\lambda i} d\lambda \simeq \lambda^* \langle \sigma_i \Phi_i \rangle / (hc)$ in m²-W⁻¹-s⁻¹ is approximately constant for each specie, given approximate spectral similarity in $F(\lambda)$ of the light sources. This means that commercially available high-intensity mercury lamps such as GE H1000 A36-15 which occupy surface areas comparable to the GE F40 BLB fluorescent bulb but emit about an order of magnitude more energy I_0 (*Black Light*, 1971), primarily in the 3200–4000 Å band, should, in principle, permit laboratory experiments with NO₂ photolysis rates as high as 3.5–5.0 min⁻¹.† As we shall see, the possibility of increasing photolysis rates by a factor of ten above typical smog chamber values has important implications for wind-tunnel simulations of photochemically reacting turbulent surface layers.

† But note that high-intensity mercury lamps emit relatively more radiation *below* 3200 Å than what penetrates to the lower atmosphere. This could lead to relative overproduction of such species as O(¹D) by O₂ + $h\nu \rightarrow$ O(¹D) + O(³P), $\lambda \leq 1750$ Å, and O₃ + $h\nu \rightarrow$ O(¹D) + O₂(¹Δ), $\lambda \leq 3100$ Å (Garvin *et al.*, 1973). To compensate, filters to remove short wavelengths below 3200 Å can be employed in a laboratory experiment.

Besides unimolecular photolysis reactions, the photochemical smog kinetic system involves both two-body ($A_i + A_j \rightarrow \text{products}$) and three-body ($A_i + A_j + A_k \rightarrow \text{products}$) collisional reactions. All three types can be written in the general form:



where subscript r denotes an individual chemical reaction in a system of M reactions, N is the total number of species participating in the system, s'_{ir} and s''_{ir} are stoichiometric coefficients of species i as a reactant and as a product respectively in reaction r and k_r is the reaction rate, temperature-dependent for collisional reactions [$k_r = k_r(T)$] and light-intensity-dependent for photolytic reactions [$k_r = J_r \tau I_0$]. (In the surface layer and in smog chambers temperature variations are sufficiently small to justify taking k_r as constants evaluated at, say, $T = 25$ C.) Summing over all reactions M , the chemical source term for species i is given by the *law of mass action*,

$$\dot{X}_i = \dot{X}_i(X_1, \dots, X_N, I_0) = \sum_{r=1}^M (s''_{ir} - s'_{ir}) k_r \prod_{i=1}^N X_i^{s'_{ir}}. \quad (9)$$

Now, in order to explore the scaling properties of the smog reactions, we consider a "nonequilibrium streamline" of constant velocity \bar{u} in the surface layer of Fig. 1. To a first approximation (neglecting vertical diffusion), the concentration variations of species i along this streamline are from (3 and 9) governed by

$$\frac{dX_i}{d(x/\bar{u})} = \sum_{r=1}^M (s''_{ir} - s'_{ir}) k_r \prod_{i=1}^N X_i^{s'_{ir}}, \quad (10)$$

where $t = x/\bar{u}$ is the reaction time in the u.v.-irradiated test section subsequent to injection of the HC/NO/NO₂ mixture through a slot near the inlet. *A fluid particle, moving along the streamline at velocity \bar{u} , experiences a local environment at distance $x = \bar{u}t$ entirely analogous to that of a particle at time t in a static smog chamber with the same initial conditions $X_i(0)$ and the same light intensity I_0 .* To express the right-hand-side of (10), it is necessary to define a specific set of photochemical smog reactions governing O₃ and PAN formation in irradiated HC/NO/NO₂ mixtures. A number of such schemes have been proposed ranging from the detailed step-by-step mechanisms of Westberg and Cohen (1970) and Niki *et al.* (1972) to the "lumped-parameter" representations of Eschenroeder and Martinez (1972) and Hecht and Seinfeld (1972). In the lumped-parameter schemes, organic radical reaction chains are represented as individual reactions which presumably reproduce the kinetic effect of the entire chain. This has the advantage of leading to more compact systems of differential equations and permits a fairly simple treatment of hydrocarbon mixtures. For our present purposes we adopt the Hecht-Seinfeld kinetic model because of its compactness, and because it has been extensively checked against smog chamber data for various hydrocarbons including propylene (or propene, C₃H₆), isobutylene, *n*-butane, propylene/*n*-butane mixtures; and, more recently (Hecht, 1972), toluene, toluene/butane, propylene/ethane and real automobile exhaust.

The Hecht-Seinfeld (1972) smog model involves 13 variable species: the primary *reactants*, nitric oxide (NO), nitrogen dioxide (NO₂) and a lumped reactive hydrocarbon (HC); the *intermediates*, nitrogen trioxide (NO₃), atomic oxygen (O), hydroxyl (OH) and hydroperoxyl (HO \dot{O}) radicals, and a lumped organic radical (RO \dot{O}) of the peroxyalkyl or peroxyacyl family; and the photochemical smog *products*, ozone (O₃), peroxyacetyl nitrates

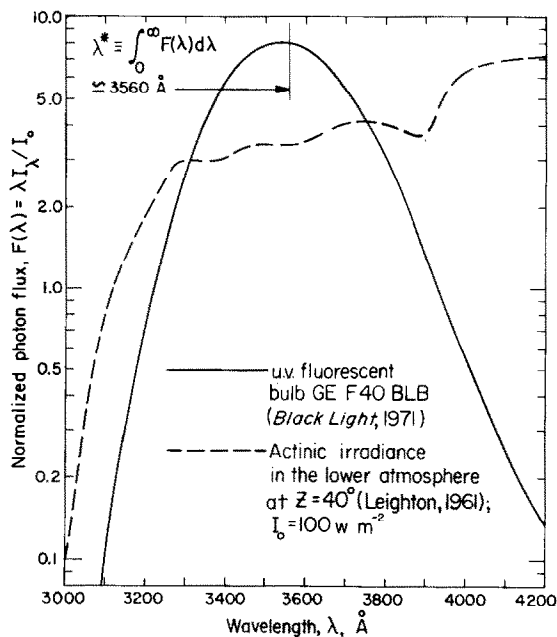


Fig. 2. Ultraviolet spectrum of normalized photon flux: The spectral properties of a light source commonly used in smog chamber experiments is compared with the estimated solar spectrum transmitted to the surface layer between 3000–4200 Å.

(PAN), nitrous (HNO_2) and nitric (HNO_3) acid, and aldehydes (RCHO). Molecular oxygen (O_2) and “air” ($M = \text{N}_2 + \text{O}_2$) do, and water vapor (H_2O) and carbon monoxide (CO) can, also participate; the concentrations of these four constituents, when present, are presumed high enough to justify taking them as sensibly constant. The evolution of smog is described in this model by a set of 15 chemical reactions reproduced here in Table 1 in which the foregoing species are active, where reactions (1 and 7) are photolytic and the rest are collisional. The characterization of organic radical reaction chains by individual reactions leads to the “effective” stoichiometric coefficients α , β , γ , δ , ϵ and θ appearing on the right-hand-sides of reactions (11–14) in this tabulation; these coefficients, as well as the rates of reactions (11–13), depend on the particular hydrocarbon or hydrocarbon mixture (HC) being modelled. Applying equation (10) to the reacting system of Table 1 leads to the set of 13 differential equations—one for each variable species—given in Table 2.

For the present study, we have developed and coded a numerical integration scheme for the GISS IBM 360/95 computer which among other things solves the Table 2 system of differential equations for the time-dependent concentrations of the variable species $X_i(t)$ starting from a prescribed initial state $X_i(0)$. [For a discussion of computational problems associated with this type of system—namely, simultaneous, “stiff” differential equations arising from disparate reaction times for the different species—see Gelinas (1972) and Eschenroeder and Martinez (1972).] Running times of this program were speeded-up by putting certain species in quasistationary states and solving for them algebraically. This is not done *a priori*, but only when right-hand-side terms are individually large but their difference, i.e. the derivative itself, is small; this condition is tested-for by the program at

Table 1. Lumped-parameter photochemical smog kinetic model for HC + NO_x + CO + H₂O systems for HC + propene (C₃H₆) adapted from Flecht and Seinfeld (1972)*

1	NO ₂ + hν → NO + O	$J_1 = 0.37 \text{ min}^{-1}$	Typical smog chamber value
2	O + O ₂ + M → O ₃ + M	$k_2 = 1.32 \times 10^{-15} \text{ ppm}^{-2} \text{ min}^{-1}$	Pseudo-first-order rate: $k_2' = [\text{O}_2][\text{M}]k_2 = 2.76 \times 10^6 \text{ min}^{-1}$
3	O ₃ + NO → NO ₂ + O ₂	$k_3 = 21.8 \text{ ppm}^{-1} \text{ min}^{-1}$	
4	O ₃ + NO ₂ → NO ₃ + O ₂	$k_4 = 6.0 \times 10^{-3} \text{ ppm}^{-1} \text{ min}^{-1}$	
5	NO _x + NO ₂ + H ₂ O → 2HNO ₃	$k_5 = 4.62 \times 10^{-6} \text{ ppm}^{-2} \text{ min}^{-1}$	
6	NO + NO ₂ + H ₂ O → 2HNO ₃	$k_6 = 1.15 \times 10^{-7} \text{ ppm}^{-2} \text{ min}^{-1}$	Pseudo-second-order rate ($\alpha, r = 0.70$): $k_5 = [\text{H}_2\text{O}]k_5 = 0.1 \text{ ppm}^{-1} \text{ min}^{-1}$
7	HNO ₃ + hν → OH + NO	$J = 5.0 \times 10^{-3} \text{ min}^{-1}$	Pseudo-second-order rate ($\alpha, r = 0.70$): $k_6 = [\text{H}_2\text{O}]k_6 = 2.5 \times 10^{-3} \text{ ppm}^{-1} \text{ min}^{-1}$
8	CO + OH + O ₂ → CO ₂ + HO ₂	$k_8 = 9.6 \times 10^{-4} \text{ ppm}^{-2} \text{ min}^{-1}$	Typical smog chamber value
9	HO ₂ + NO → NO ₂ + OH	$k_9 = 1.8 \times 10^5 \text{ ppm}^{-2} \text{ min}^{-1}$	Pseudo-second-order rate: $k_8 = [\text{O}_2]k_8 = 2.0 \times 10^6 \text{ ppm}^{-1} \text{ min}^{-1}$
10	HO ₂ + NO ₂ → HNO ₃ + O	$k_{10} = 10.0 \text{ ppm}^{-2} \text{ min}^{-1}$	
11	HC + O → zRO ₂	$k_{11} = 5.0 \times 10^4 \text{ ppm}^{-1} \text{ min}^{-1}$	
12	HC + O ₃ → βRO ₂ + γRCHO	$k_{12} = 7.5 \times 10^{-3} \text{ ppm}^{-1} \text{ min}^{-1}$	$z = \frac{2.48[\text{NO}][\text{HC}]}{9.8 \times [\text{NO}][\text{HC}] + 0.25 \times [\text{NO}][\text{HC}]^{0.5}}$
13	HC + OH → δRO ₂ + εRCHO	$k_{13} = 1.0 \times 10^5 \text{ ppm}^{-1} \text{ min}^{-1}$	$\beta = 1.7, \gamma = 9$
14	RO ₂ + NO → NO ₂ + R ₂ OH	$k_{14} = 1.8 \times 10^5 \text{ ppm}^{-1} \text{ min}^{-1}$	$\delta = 0.8, \epsilon = 2$
15	RO ₂ + NO ₂ → PAN	$k_{15} = 10.0 \text{ ppm}^{-1} \text{ min}^{-1}$	$\theta = 0.02$

* Ambient background concentrations at 25°C: [O₂] = 2.09 × 10⁵ ppm, [M] = 1.00 × 10⁶ ppm, [H₂O] = (3.1 × 10⁴) × *r* ppm, where *r* = r.h.

Table 2. Chemical source terms $\dot{X}_i = \dot{X}_i(X_1, \dots, X_N)$ (ppm-min⁻¹)

1	$d[\text{NO}]/dt = J_1[\text{NO}_2] - k_3[\text{O}_3][\text{NO}] - k_6[\text{NO}][\text{NO}_2][\text{H}_2\text{O}] + J_7[\text{HNO}_2]$ $- k_9[\text{HO}\dot{\text{O}}][\text{NO}] - k_{14}[\text{RO}\dot{\text{O}}][\text{NO}]$
2	$d[\text{NO}_2]/dt = -J_1[\text{NO}_2] + k_3[\text{O}_3][\text{NO}] - k_4[\text{O}_3][\text{NO}_2] - k_5[\text{NO}_3][\text{NO}_2][\text{H}_2\text{O}]$ $- k_6[\text{NO}][\text{NO}_2][\text{H}_2\text{O}] + k_9[\text{HO}\dot{\text{O}}][\text{NO}] - k_{10}[\text{HO}\dot{\text{O}}][\text{NO}_2]$ $+ k_{14}[\text{RO}\dot{\text{O}}][\text{NO}] - k_{15}[\text{RO}\dot{\text{O}}][\text{NO}_2]$
3	$d[\text{HC}]/dt = -k_{11}[\text{HC}][\text{O}] - k_{12}[\text{HC}][\text{O}_3] - k_{13}[\text{HC}][\text{OH}]$
4	$d[\text{O}_3]/dt = k_2[\text{O}][\text{O}_2][\text{M}] - k_3[\text{O}_3][\text{NO}] - k_4[\text{O}_3][\text{NO}_2] - k_{12}[\text{HC}][\text{O}_3]$
5	$d[\text{O}]/dt = J_1[\text{NO}_2] - k_2[\text{O}][\text{O}_2][\text{M}] - k_{11}[\text{HC}][\text{O}]$
6	$d[\text{NO}_3]/dt = k_4[\text{O}_3][\text{NO}_2] - k_5[\text{NO}_3][\text{NO}_2][\text{H}_2\text{O}]$
7	$d[\text{OH}]/dt = J_7[\text{HNO}_2] - k_8[\text{CO}][\text{OH}][\text{O}_2] + k_9[\text{HO}\dot{\text{O}}][\text{NO}] - k_{13}[\text{HC}][\text{OH}]$ $+ \theta k_{14}[\text{RO}\dot{\text{O}}][\text{NO}]$
8	$d[\text{HO}\dot{\text{O}}]/dt = k_8[\text{CO}][\text{OH}][\text{O}_2] - k_9[\text{HO}\dot{\text{O}}][\text{NO}] - k_{10}[\text{HO}\dot{\text{O}}][\text{NO}_2]$
9	$d[\text{RO}\dot{\text{O}}]/dt = \alpha k_{11}[\text{HC}][\text{O}] + \beta k_{12}[\text{HC}][\text{O}_3] + \delta k_{13}[\text{HC}][\text{OH}] - k_{14}[\text{RO}\dot{\text{O}}][\text{NO}]$ $- k_{15}[\text{RO}\dot{\text{O}}][\text{NO}_2]$
10	$d[\text{HNO}_2]/dt = 2k_6[\text{NO}][\text{NO}_2][\text{H}_2\text{O}] - J_7[\text{HNO}_2] + k_{10}[\text{HO}\dot{\text{O}}][\text{NO}_2]$
11	$d[\text{HNO}_3]/dt = 2k_4[\text{NO}_3][\text{NO}_2][\text{H}_2\text{O}]$
12	$d[\text{RCHO}]/dt = \gamma k_{12}[\text{HC}][\text{O}_3] + \epsilon k_{13}[\text{HC}][\text{OH}]$
13	$d[\text{PAN}]/dt = k_{15}[\text{RO}\dot{\text{O}}][\text{NO}_2]$

appropriate computational steps. Ideally we would like to use the computer model to show that by varying controllable factors such as light intensity I_0 and initial reactant concentrations $X_i(0)$ it is possible to generate smog distributions along nonequilibrium wind-tunnel turbulent shear layer streamlines which are scaled versions of those in smog chambers and urban atmospheres.

Because the photochemical smog system is a combination of unimolecular, bimolecular and termolecular reactions which (as a result of the "constant" species O_2 , M , H_2O and CO) acts as a combination of effectively first- and second-order reactions it is not obvious that this system obeys a simple scaling law which collapses the distributions at different values of I_0 and $X_i(0)$ to a single curve. But we found from numerical experiments with the computer model and starting from a smog-chamber-validated ($\text{HC} = \text{propylene}$) distribution discussed by Hecht and Seinfeld (1972) that an *approximate* scaling law of this type does, in fact, exist. At the reference conditions, the initial concentrations are $X_{\text{NO}}^*(0) = 1.612$ ppm, $X_{\text{NO}_2}^*(0) = 0.088$ ppm and $X_{\text{HC}}^*(0) = 3.29$ ppm for the primary reactants, the initial concentrations of the other variable species is zero, the relative humidity is $r = 0.7$ (see Table 1) and $X_{\text{CO}}^* = 0$. For these conditions and the rate coefficients of Table 1 we computed time-dependent distributions of NO , NO_2 , HC and O_3 practically indistinguishable from those given in Hecht and Seinfeld (1972), despite some differences in the numerical integration schemes.

Smog chamber experiments typically exhibit initial *incubation* regimes beginning immediately after the u.v. lights are turned on wherein NO is first converted into NO_2 , followed by *ozone-formation* regimes beginning shortly after the incubation time τ at which NO_2 reaches its maximum concentration. For concentration levels and light intensities commonly used in smog chambers the incubation time for $\text{HC} = \text{propylene}$ is of the order of 1 h ($\tau^* \simeq 70$ min for the Hecht-Seinfeld reference condition). To study the scaling properties of smog, we normalized the reaction time by the incubation time τ and normalized all concentrations by the initial nitric oxide concentration $X_{\text{NO}}(0)$. For the reference conditions the computed distributions of NO , NO_2 , HC and O_3 , so-normalized, are illustrated by the solid curves in Fig. 3. Significantly, we found that scaling J_1 , J_7 , $X_{\text{NO}}(0)$, $X_{\text{NO}_2}(0)$ and $X_{\text{HC}}(0)$ up by a factor of ten resulted in *normalized* distributions very nearly

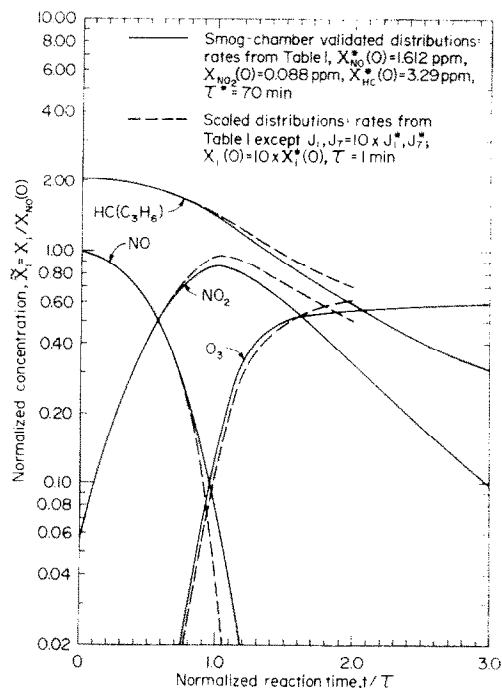


Fig. 3. Comparison of normalized smog distributions obtained from computer model at two different experimental conditions. The distributions are approximately collapsed by this normalization although the scaled (dashed) distributions are "faster" by a factor of 70.

coincident with those of the reference conditions, as shown by the dashed curves in Fig. 3; although here, the peak occurred at $\tau \approx 1$ min. We must note that this scaling appears, at present, to be only approximate and that further theoretical and experimental work is needed to establish scaling regimes more rigorously; the indications are that incubation and ozone-formation regimes may scale in slightly different ways.† Nonetheless, these results are of great importance in the present context because they suggest that ozone formation times can be reduced to the order of one minute while preserving very nearly the same distribution found in smog chambers simply by increasing initial primary reactant concentrations and light intensities by an order of magnitude. This should be within the state of the art (see prior discussion).

In wind-tunnel simulations, fluid particle residence times are determined by the minimum freestream velocity required for a (Reynolds-number-independent) turbulent shear layer, roughly $u_0 \sim 1.3 \text{ m s}^{-1}$ ($\sim 1 \text{ ft s}^{-1}$), and the nominal test-section length, say $L \sim 10$ m, so that $\tau_r = L/u_0 \sim 0.5$ min is a reasonable value. To form ozone within this test section requires formation times of the same order but about a factor of two faster than that of the scaled distribution in Fig. 3. This additional acceleration of the chemistry can be accomplished in several ways: by raising I_0 , by using a more reactive hydrocarbon such as *trans*-2-butene (Eschenroeder and Martinez, 1972), or by increasing the initial concentration ratio of nitrogen dioxide to nitric oxide $X_{\text{NO}_2}(0)/X_{\text{NO}}(0)$. As suggested by the computer sensitivity studies of Niki *et al.* (1972), the latter tends to shorten the incubation time so that ozone

† Also, in the absence of experimental data, we cannot entirely exclude the possibility of a change in kinetic mechanism at these higher concentrations.

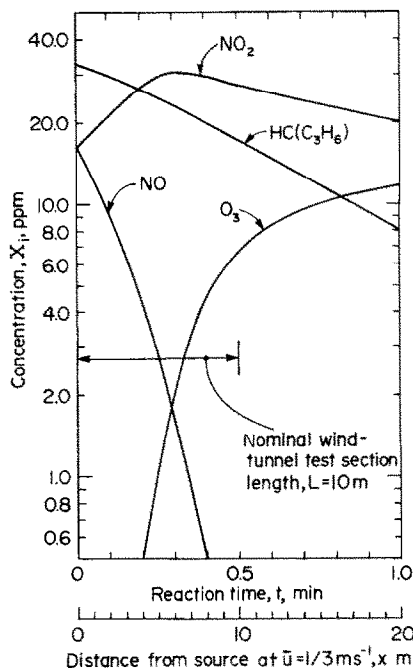


Fig. 4. Computed photochemical smog species along a nonequilibrium boundary-layer streamline (neglecting diffusion) for $J_1 = 3.7 \text{ min}^{-1}$, $J_7 = 5 \times 10^{-2}$ ($I_0 = 10 \times I_0^*$), $X_{\text{NO}}(0) = X_{\text{NO}_2}(0) = 16.12$ and $X_{\text{HC}}(0) = 32.9$ ppm. Note the formation of most of the ozone over the first 10 m, the nominal length of the wind tunnel test section in the proposed experiment.

is formed earlier. In Fig. 4, we show the results of a computer simulation based on this principle, namely, where all experimentally controllable parameters are the same as those of the scaled Fig. 3 distribution except that $X_{\text{NO}_2}(0) = X_{\text{NO}}(0) = 16.12$ ppm. As depicted in Fig. 4 this results in an incubation time of $\tau \sim 0.3$ min and an O_3 -distribution for which most of the ultimate ozone is formed within the first 1/2 min, as required for the wind-tunnel simulations of turbulent, photochemically reacting surface layers.

DISCUSSION

The foregoing considerations indicate the feasibility of scale modelling the *coupled* fluid dynamic and photochemical effects active in photochemical smog formation by exploiting, in combination, certain wind tunnel and smog chamber techniques already used to study these effects separately. Operationally, the success of such a facility depends on achieving the conditions needed for both fluid dynamic and photochemical similitude in turbulent shear layers generated over a u.v.-irradiated test section. Accordingly, it seems appropriate here to discuss some practical questions arising in the design of this type of laboratory experiment.

It is envisioned that *laboratory* feasibility would be demonstrated initially most economically in a facility adapted from a pre-existing "air pollution" wind tunnel by adding banks of high-intensity mercury vapor lamps separated from the main flow by a u.v.-transparent sheet as illustrated in Fig. 1. For a 10 m long test section, we estimate that at least one hundred (possibly more, depending on test section width) 1000 W high-intensity mercury lamps will be needed to get radiation levels up to the point where ozone is formed

in the test section. Most of this 100 kW of energy will be dissipated as heat at the lamps themselves so that some cooling—either from bypassing the main flow or from separate blowers—will probably be needed. On the other hand, a steady state should be attained within a few minutes after the lamps come up to full intensity so the total energy expended on any given experiment will not be excessive. (Actually, in the photochemical scaling discussed previously the product of radiation intensity and reaction time *decreases* with increasing light intensity.)

Initial concentrations of the primary reactants required to form test section ozone could be readily attained by creating an NO/NO₂/HC premixture from bottled gases in a plenum chamber and injecting this into the slot at appropriate flow-rates. Concentration levels needed for these experiments are several orders of magnitude above urban atmosphere levels (Larson, 1971) and about one order of magnitude above smog chamber levels. Because of the possibility of scaling the concentration fields, this need not detract from the realism or applicability of these experiments and is actually an advantage for several reasons. For example, the high reactant and product concentrations mean that impurities and trace gases in the background air (essentially urban in open-circuit tunnels) and wall effects on the chemistry are relatively less important than in smog chambers. Also, the sensitivity of concentration-measuring instruments is generally much greater at higher concentrations and some constituents cannot be detected at all below certain instrumental thresholds.

With regard to the instrumentation, it is desirable that turbulent-mean concentrations of at least NO, NO₂, HC, O₃ and PAN be mapped as a function of position in the steady state; if possible the fluctuating components should be measured as well to assess the importance of correlation terms of the form $\overline{X_i'X_j'}$ which strictly speaking appear in the turbulent-mean chemical source term (Hoffert, 1972). A number of well-developed techniques are available for monitoring concentrations based on analysis of samples removed from the flow (Butcher and Charlson, 1972). This type of experiment also lends itself to various types of remote sensing instrumentation including laser transmissometers, laser Raman scattering devices and correlation spectrometers. Indeed, the proposed facility could serve as a nearly ideal test bed for these instruments over a controlled, turbulent, chemically reacting environment because the high concentrations should provide appreciable column thicknesses, $I = \int_0^L X_i ds$, where s is the path length of the light beam, despite physical dimensions which are smaller than those in the field. To characterize the momentum and energy distributions in the shear layer it will be necessary also to monitor the velocity and temperature fields, including if possible the fluctuating components, using the standard hot-wire anemometer, pressure-traverse and thermocouple instrumentation of the low-speed aerodynamicist.

Although we have not specifically discussed the formation of aerosol particles in smog or the effects of CO and SO₂ on smog formation and vice versa, these phenomena too appear amenable to study in the proposed facility because their characteristic reaction times are controlled by oxidant (or ozone) formation times.

To summarize, it appears from our preliminary study that a hybrid wind-tunnel smog-chamber facility of the type described here is feasible and could provide data of a unique type on fundamental interactions between turbulent atmospheric surface layers and the smog chemistry within them. This data, in turn, should facilitate the resolution of questions relating to mathematical models for the dispersal of chemically reacting air pollutants, permit a check of these models under controlled conditions, serve as a simulation

of the urban polluted atmosphere itself and, hopefully, shed new light on this murky subject.

Acknowledgements—Two of us (M.I.H. and S.H.) wish to acknowledge the support of the National Academy of Sciences in the form of Senior Resident Research Associateships at the Institute for Space Studies, Goddard Space Flight Center, National Aeronautics and Space Administration, New York, New York.

REFERENCES

- Air Quality Criteria for Hydrocarbons* (1970) National Air Pollution Control Administration Publication No. AP-64, U.S. Government Printing Office, Washington, D.C.
- Air Quality Criteria for Nitrogen Oxides* (1971) Environmental Protection Agency, Air Pollution Control Office Publication No. AP-84, U.S. Government Printing Office, Washington, D.C.
- Air Quality Criteria for Photochemical Oxidants* (1970) National Air Pollution Control Administration Publication No. AP-63, U.S. Government Printing Office, Washington, D.C.
- Black Light* (1971) General Electric Technical Publication No. 125, General Electric Company, Large Lamp Department, Nela Park, Cleveland, Ohio.
- Butcher S. S. and Charlson R. J. (1972) *An Introduction to Air Chemistry*. Academic Press, New York.
- Cermak J. E. (1971) Laboratory simulation of the atmospheric boundary layer. *AIAA J.* **9**(9), 1746–1754.
- Cook N. J. (1973) On simulating the lower third of the urban adiabatic boundary layer in a wind tunnel. *Atmospheric Environment* **7**(7), 691–705.
- Counihan J. (1973) Simulation of an adiabatic urban boundary layer in a wind tunnel. *Atmospheric Environment* **7**(7), 673–689.
- Dodge M. C. and Bufalini J. J. (1972) The role of carbon monoxide in polluted atmospheres. In *Photochemical Smog and Ozone Reactions*, (Edited by R. F. Gould, pp. 232–245. Advances in Chemistry Series 113, American Chemical Society, Washington, D.C.
- Donaldson C. duP. and Hilst G. R. (1972) Effect of inhomogeneous mixing on atmospheric photochemical reactions. *Environ. Sci. Technol.* **6**(9), 812–816.
- Eschenroeder A. Q. and Martinez J. R. (1972) Concepts and applications of photochemical smog models. In *Photochemical Smog and Ozone Reactions*, (Edited by R. F. Gould, pp. 101–168. Advances in Chemistry Series 113, American Chemical Society, Washington, D. C.
- Garvin D., Herron J. T., Huie R. E., Kurylo M. J., Laufer A. H., Okabe H., Scheer M. D. and Tsang W. (1973) *Chemical Kinetics Data Survey VI: Photochemical and Rate Data for Twelve Gas Phase Reactions of Interest for Atmospheric Chemistry*, (Edited by R. F. Hamson) Document No. NBSIR 73–207, Physical Chemistry Division, Institute for Materials Research, National Bureau of Standards, Washington, D.C.
- Gelinas R. J. (1972) Stiff systems of kinetic equations—a practitioner's view. *J. Comput. Phys.* **9**, 222–236.
- Hecht T. A. (1972) Further validation of a generalized mechanism suitable for describing atmospheric photochemical reactions. Appendix B of Report 72-SAI-26, prepared by Systems Applications, Inc., Beverly Hills, California, for the U.S. Environmental Protection Agency, Research Triangle Park, North Carolina.
- Hecht T. A. and Seinfeld J. H. (1972) Development and validation of a generalized mechanism for photochemical smog. *Environ. Sci. Technol.* **6**(1), 47–57.
- Hoffert M. I. (1972) Atmospheric transport, dispersion and chemical reactions in air pollution: a review. *AIAA J.* **10**(4), 377–387.
- Hoydysh W. G. and Ogawa Y. (1972a) Characteristics of wind turbulence and pollutant concentration in and above a model city. Report No. EERL NYU 110, Environmental Engineering Research Laboratories, New York University, Bronx, New York.
- Hoydysh W. G. and Ogawa Y. (1972b) A two-dimensional study of dispersion of automotive pollution in street canyons. Report No. EERL NYU 111, Environmental Engineering Research Laboratories, New York University, Bronx, New York.
- Jensen M. (1958) The model-law for phenomena in natural wind. *Ing. Int. Ed.* **2**(4), 121–128.
- Kolmogorov A. N. (1941) The local structure of turbulence in an incompressible fluid for very large wavenumbers. *Proceedings (Dokl.) Acad. Sci., U.S.S.R.* **30**, 301–305.
- Lamb R. G. (1973) Note on the application of *K*-theory to diffusion problems involving nonlinear chemical reactions. *Atmospheric Environment* **7**, 257–263.
- Lamb R. G. and Seinfeld J. H. (1973) Mathematical modeling of urban air pollution: general theory. *Environ. Sci. Technol.* **7**(3), 253–261.
- Larson R. I. (1971) A mathematical model for relating air quality measurements to air quality standards. EPA Office of Air Programs Publication No. AP-89, U.S. Environmental Protection Agency, Research Triangle Park, North Carolina.
- Leighton P. A. (1961) *Photochemistry of Air Pollution*. Academic Press, New York.
- Monin A. S. and Yaglom A. M. (1971) *Statistical Fluid Mechanics: Mechanics of Turbulence*, (Edited by J. L. Lumley) Vol. 1, pp. 417–526. MIT Press, Cambridge, Massachusetts.

- Niki H., Daby E. E. and Weinstock B. (1972) Mechanisms of smog reactions. In *Photochemical Smog and Ozone Reactions*, (Edited by R. F. Gould), pp. 16-57. Advances in Chemistry Series 113, American Chemical Society, Washington, D.C.
- Seinfeld J. H., Reynolds S. D. and Roth P. M. (1972) Simulation of urban air pollution. In *Photochemical Smog and Ozone Reactions*, (Edited by R. F. Gould), pp. 58-100. Advances in Chemistry Series 113, American Chemical Society, Washington, D.C.
- Snyder W. H. (1972) Similarity criteria for the application of fluid models to the study of air pollution meteorology. *Boundary Layer Met.* **3**(1), 113-134.
- Sundaram T. R., Ludwig G. R. and Skinner G. T. (1972) Modeling the turbulence structure of the atmospheric surface layer. *AIChE J.* **10**(6), 743-750.
- Tennekes H. and Lumley J. L. (1972) *A First Course in Turbulence*. MIT Press, Cambridge, Massachusetts.